Electronic Supplementary Material (ESI) for Physical Chemistry Chemical Physics.

Supporting information for:

Three-dimensional docking of alcohols to ketones: An experimental benchmark based on acetophenone solvation energy balances

C. Zimmermann, H. C. Gottschalk, M. A. Suhm*

E-mail: msuhm@gwdg.de

Table S1: ORCA[S1,S2], Gaussian Rev. E.01[S3] and TURBOMOLE[S4,S5] keywords used for the different optimizations and the transition state search (TS).

Level of approximation	Employed keywords
B3LYP-D3(BJ,ABC)/def2-TZVP* (ORCA)	B3LYP D3BJ def2-TZVP abc grid5 NoFinalGrid UseSym VERYTIGHTSCF TIGHTOPT FREQ
DLPNO-CCSD(T) (ORCA)	DLPNO-CCSD(T) TightPNO aug-cc-pVQZ aug-cc-pVQZ/C TightSCF LED
TPSS-D3(BJ,ABC)/def2-TZVP* (ORCA)	TPSS D3BJ def2-TZVP abc grid5 NoFinalGrid UseSym VERYTIGHTSCF TIGHTOPT NumFreq
B97-3c (ORCA)	B97-3c GRID5 NOFINALGRID VERYTIGHTSCF TIGHTOPT FREQ
PBEh-3c (ORCA)	PBEH-3c GRID5 NOFINALGRID VERYTIGHTSCF TIGHTOPT FREQ
M06-2X (Gaussian)	m062x def2TZVP opt=tight scf=tight Integral(Grid=UltraFineGrid) freq
B97-3c-D3(BJ,ABC)/def2-mTZVP (TURBOMOLE)[TS]	b973c def2-mTZVP grid m5 disp3 bj abc ri itrvec 1
B3LYP-D3(BJ,ABC)/def2-TZVP (ORCA)[TS]	B3LYP D3BJ def2-TZVP abc grid5 NoFinalGrid UseSym OptTS VERYTIGHTSCF TIGHTOPT FREQ

*Additional single point calculation with def2-QZVP.

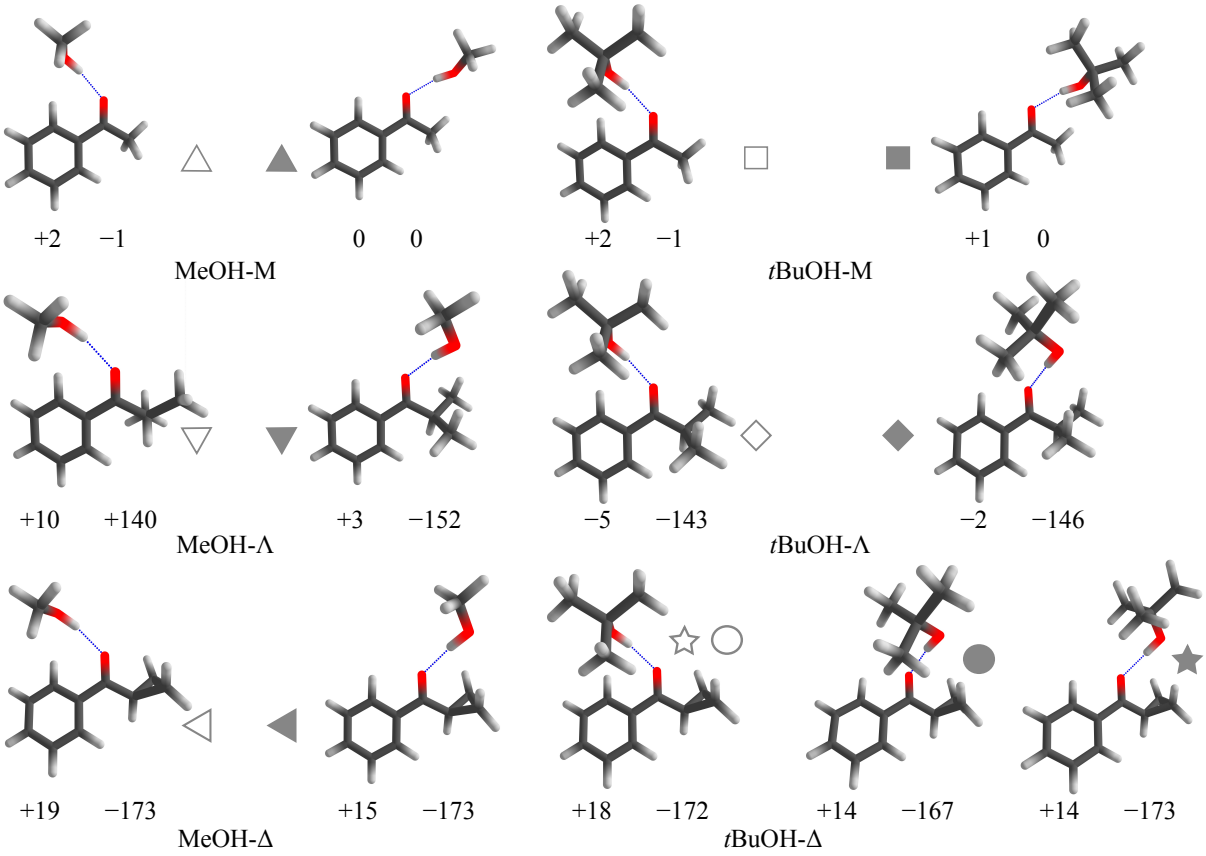

Fig. S1: Structures of the most stable alcohol/acetophenone derivative dimers at B3LYP-D3(BJ,abc)/def2-TZVP level together with the symbols used for them in the main text, with the solvating alcohol residue pointing towards the reader. Also given are the torsional angles relative to the ketone group on the phenyl side (CC-CO, left value; if positive, the CO group points more to the reader than the nearly parallel phenyl CH group in ortho position) and on the alkyl side (OC-CH, right value; if positive, the CH closest to the ketone plane points towards the reader) in ° for the complex structures. The corresponding values for the isolated ketones are for M $0°$ and $0°$, for Λ $+4°$ and $+143°$, for Δ $+13°$ and $-173°$.

Table S2: Alkyl coordination energies of acetophenone derivative/MeOH and *t*BuOH complexes predicted by different quantum-chemical calculations in $\mathrm{kJ\,mol^{-1}}$ relative to the phenyl coordination. ΔE^{el} excludes and ΔE^{0} includes the harmonically approximated zero-point energy. Positive energy differences denote a higher stability of the complex where the solvent docks on the phenyl side. Zero-point energy does not change the energy sequence and typically causes a small correction.

Acceptor	Method	MeOH		*t*BuOH	
		$\Delta E^{\mathrm{el}}_{\mathrm{R-Ph}}$	$\Delta E^{0}_{\mathrm{R-Ph}}$	$\Delta E^{\mathrm{el}}_{\mathrm{R-Ph}}$	$\Delta E^{0}_{\mathrm{R-Ph}}$
M	B3LYP-D3(BJ)	-0.5	-0.6	-0.2	-0.2
	TPSS-D3(BJ)	-0.9	-1.0	-0.5	-0.5
	M06-2X	-0.5	-0.3	-0.9	-0.5
	B97-3c	-1.2	-1.3	-0.9	-0.9
	PBEh-3c	-0.6	-0.5	-0.6	-0.6
Λ	B3LYP-D3(BJ)	-0.1	-0.2	-1.2	-0.9
	TPSS-D3(BJ)	-0.1	0.0	-0.7	-0.7
	M06-2X	-1.5	-1.5	-1.7	-1.6
	B97-3c	-0.4	-0.4	-1.1	-0.8
	PBEh-3c	$+1.0$	$+0.9$	-0.3	-0.4
Δ	B3LYP-D3(BJ)	$+1.3$	$+0.7$	$+0.3$	$+0.2$
	TPSS-D3(BJ)	$+1.1$	$+0.4$	$+0.3$	$+0.4$
	M06-2X	$+1.0$	$+0.4$	$+0.2$	$+0.5$
	B97-3c	$+1.2$	$+0.5$	$+0.4$	$+0.5$
	PBEh-3c	$+2.1$	$+1.6$	$+1.1$	$+0.8$
'-Δ	B3LYP-D3(BJ)			$+0.8$	$+0.6$
	TPSS-D3(BJ)			$+0.3$	$+0.5$
	M06-2X			-0.1	$+0.5$

Table S3: Docking effect on the harmonic OH stretching wavenumbers ω and resulting wavenumber splittings $\Delta\omega$ for alkyl (R) and phenyl (Ph) docking variants of acetophenone derivative/MeOH and *t*BuOH complexes in cm^{-1}. Negative signs indicate a higher wavenumber for phenyl docking and allow for an assignment of the Δ' complex with *t*BuOH.

Acceptor	Method	MeOH			*t*BuOH		
		ω		$\Delta\omega_{\mathrm{R-Ph}}$	ω		$\Delta\omega_{\mathrm{R-Ph}}$
		R	Ph		R	Ph	
M	B3LYP-D3(BJ)	3619	3664	−44	3616	3656	−40
	TPSS-D3(BJ)	3476	3528	−52	3469	3514	−45
	M06-2X	3763	3801	−39	3731	3767	−37
	B97-3c	3560	3611	−51	3555	3603	−49
	PBEh-3c	3840	3871	−30	3820	3849	−29
Λ	B3LYP-D3(BJ)	3632	3664	−32	3649	3657	−8
	TPSS-D3(BJ)	3497	3527	−31	3510	3515	−5
	M06-2X	3809	3800	+10	3763	3773	−9
	B97-3c	3566	3607	−41	3589	3603	−14
	PBEh-3c	3863	3870	−8	3846	3846	0
Δ	B3LYP-D3(BJ)	3629	3648	−20	3661	3640	+21
	TPSS-D3(BJ)	3493	3510	−17	3520	3491	+28
	M06-2X	3735	3785	−50	3777	3738	+40
	B97-3c	3573	3589	−16	3608	3571	+37
	PBEh-3c	3862	3858	+4	3836	3839	−4
’-Δ	B3LYP-D3(BJ)				3625	3640	−15
	TPSS-D3(BJ)				3480	3491	−11
	M06-2X				3736	3738	−2

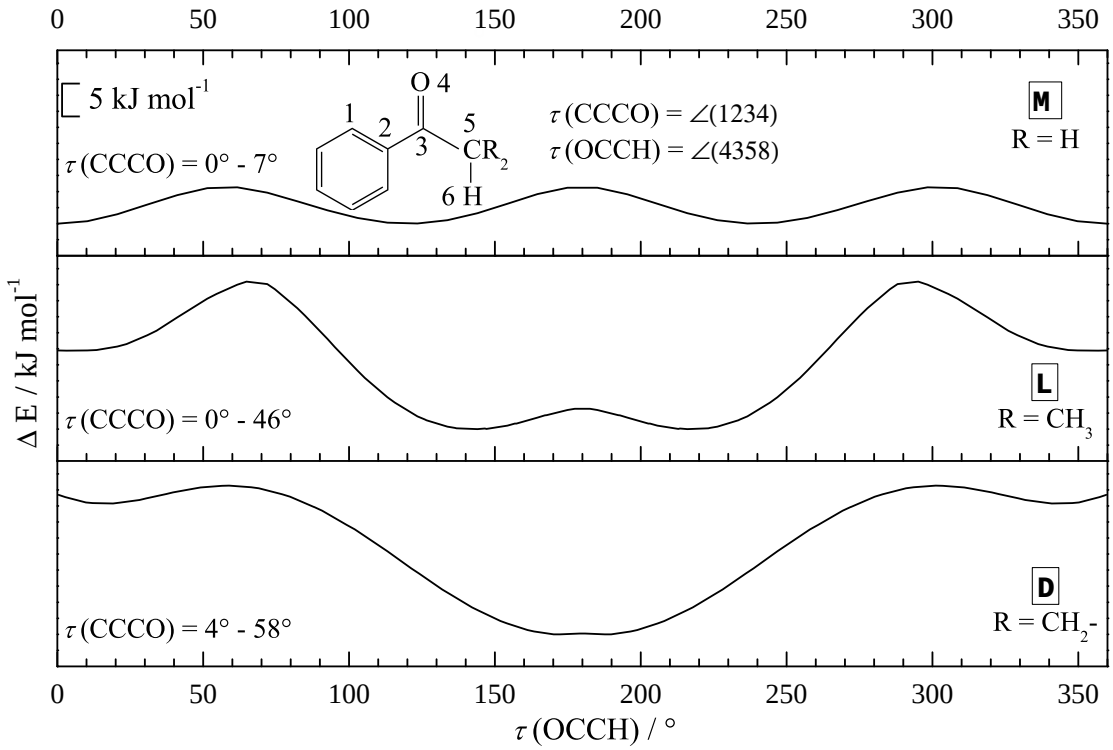

Fig. S2: Relaxed B3LYP-D3(BJ,ABC)/def2-TZVP scans along the aliphatic OCCH torsional angle for acetophenone M (with minima at $0°$, $120°$, $240°$) and its derivatives Λ (with two equivalent structures at $(180 \pm 37)°$) and Δ (with two equivalent structures at $(180 \pm 7)°$). Barriers below $5\,\mathrm{kJ\,mol^{-1}}$ (see insert) can be largely overcome in jet expansions, such that higher lying minima should relax to the lowest energy structure (Δ) and in any case be rather weakly populated from the start at room temperature (Λ, Δ). The relaxation is associated with major rearrangements of the aromatic CC-CO torsional angle for the more bulky systems (the angle range is indicated in the individual panels). Based on these predictions, no major monomer isomerism should be observed in the spectra. However, a docking alcohol molecule encounters very different environments on the aliphatic side. For M, there is a C-H bond in the carbonyl plane, for Λ it meets two unsymmetrically tilted methyl groups and for Δ the cyclopropyl ring shields the C=O group rather symmetrically. This modulates the accessibility of the aliphatic lone pair of the keto group.

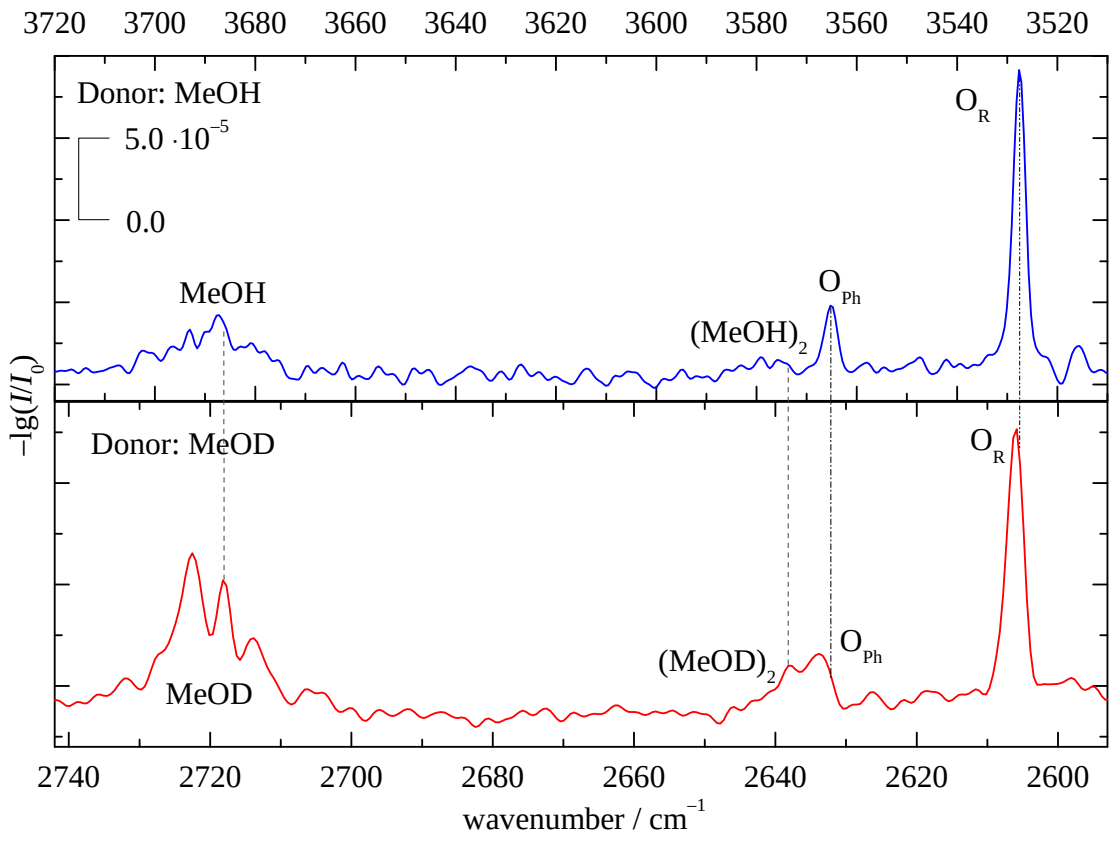

Fig. S3: Comparison of the spectra for M with MeOH and MeOD after stretching the OD wavenumber axis by $\sqrt{2}$ and matching the two monomer transitions at $3686\,\mathrm{cm}^{-1}$ and $2718\,\mathrm{cm}^{-1}$. The close analogy (visualized by vertical dashed lines) confirms an insignificant influence of zero-point energy on the energy difference between the two docking variants.

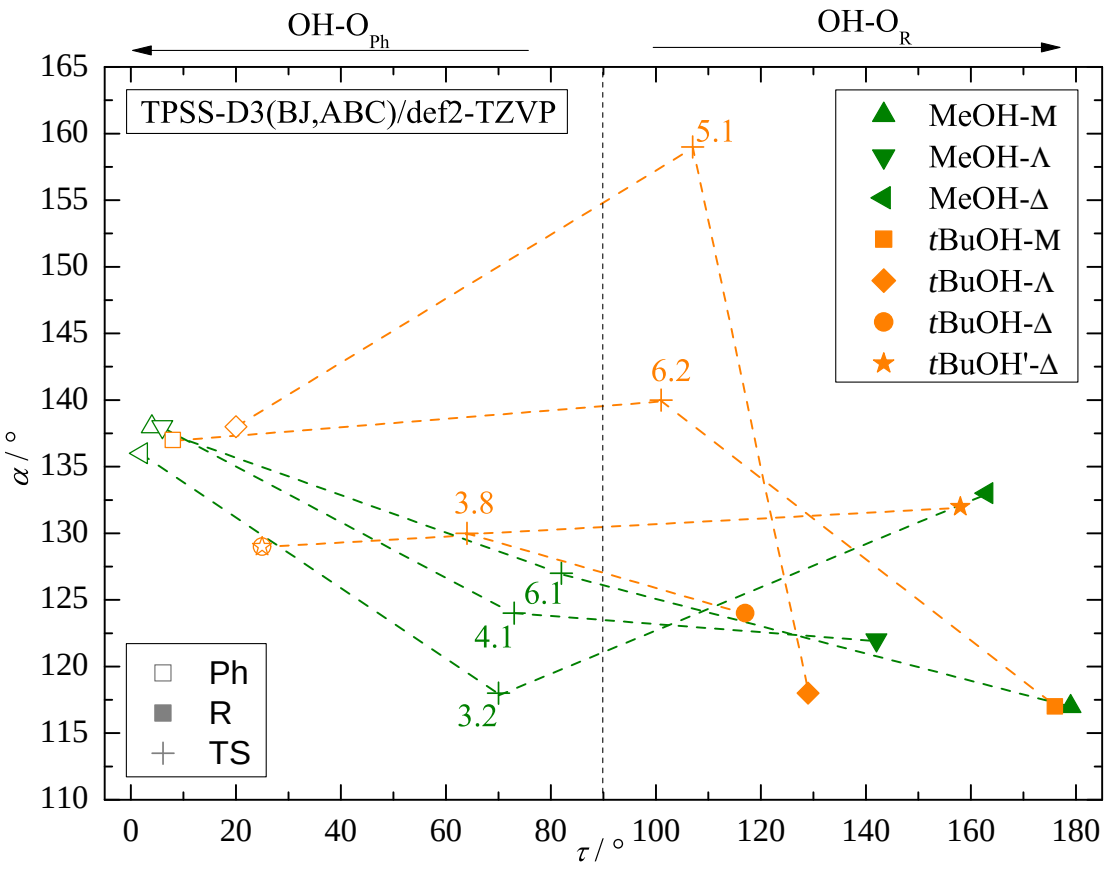

Fig. S4: TPSS structural predictions for the phenyl-to-alkyl (Ph-to-R, left-to-right) docking switch in terms of hydrogen bond angle α and out-of-plane twist τ for the six combinations of ketone and alcohol. Transition state barriers form the phenyl side in $\mathrm{kJ\,mol^{-1}}$ are placed near their location (+).

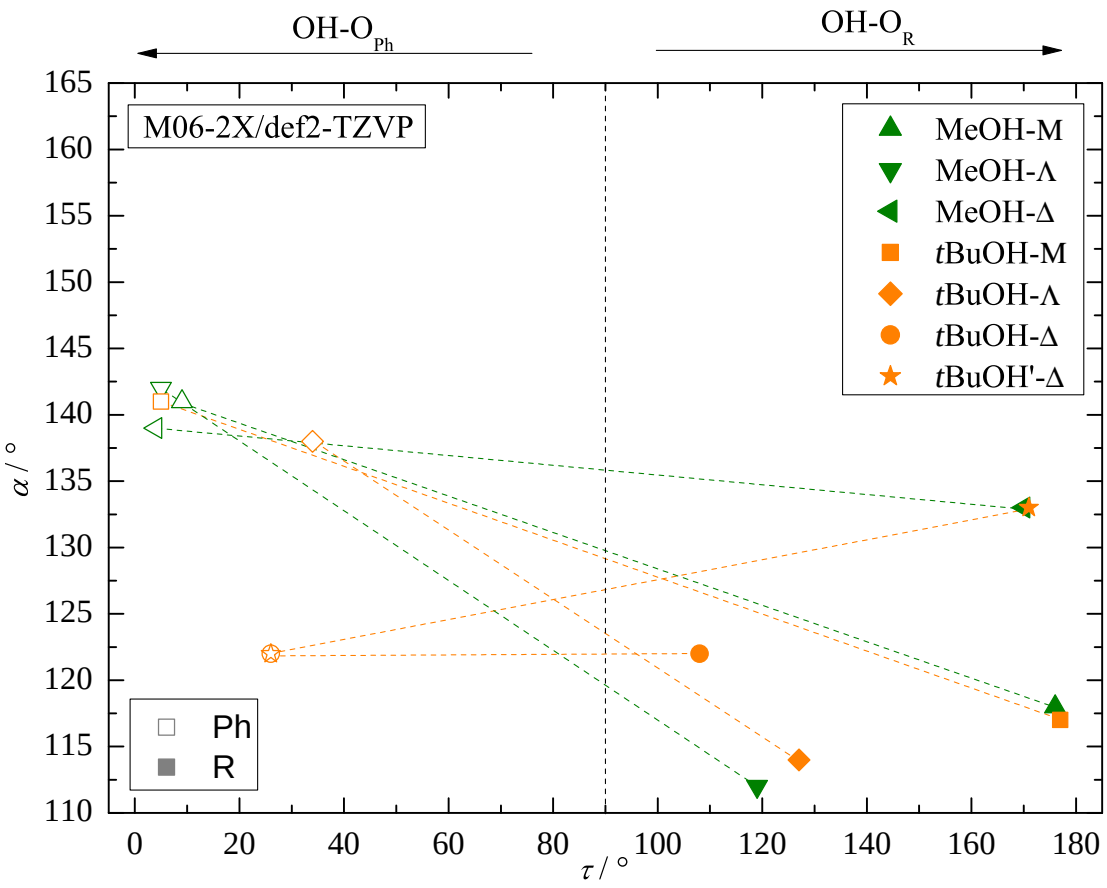

Fig. S5: M06-2X structural predictions for the phenyl-to-alkyl (Ph-to-R, left-to-right) docking switch in terms of hydrogen bond angle α and out-of-plane twist τ for the six combinations of ketone and alcohol.

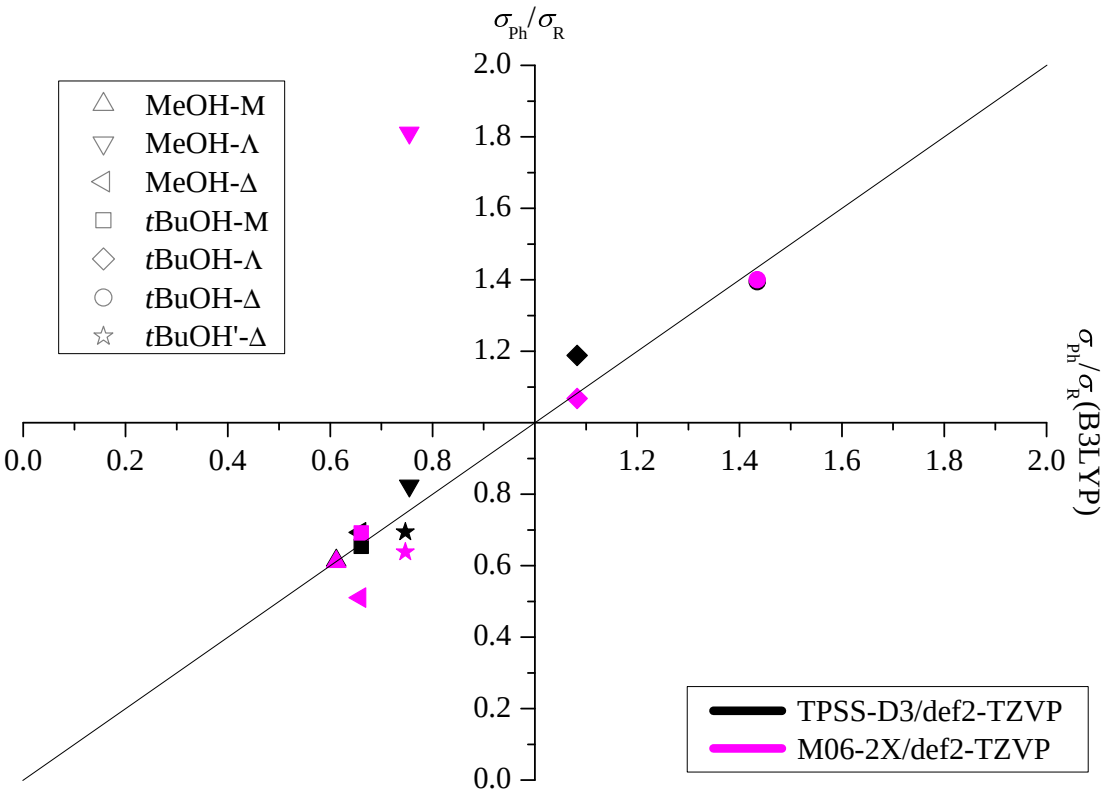

Fig. S6: TPSS and M06-2X infrared band strength ratios $\sigma_{\mathrm{Ph}}/\sigma_{\mathrm{R}}$ plotted against the B3LYP infrared band strength ratios.

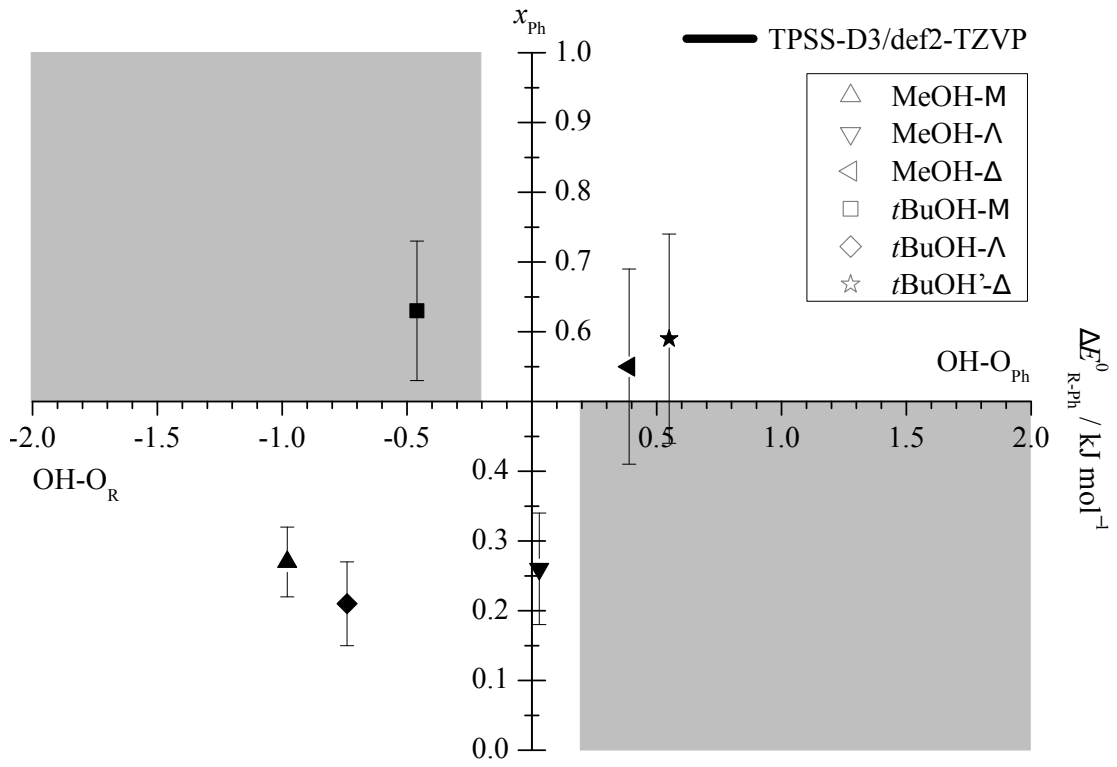

Fig. S7: Experimental fraction of phenyl docking $x_{\mathrm{Ph}} = c_{\mathrm{Ph}}/(c_{\mathrm{R}} + c_{\mathrm{Ph}})$ plotted against the TPSS-predicted ZPV corrected energy advantage for phenyl docking $\Delta E^0_{\mathrm{R-Ph}}$. Allowing for an estimated error of the ZPV correction of $\pm 0.2\,\mathrm{kJ\,mol^{-1}}$, grey areas should not fully contain data points within their indicated experimental integration error bar, if relative absorption cross sections calculated at the same level are reliable. This is the case for all systems except for *t*BuOH-M, where TPSS predicts a slight alkyl-docking preference but the spectral intensity is consistent with more phenyl-docking.

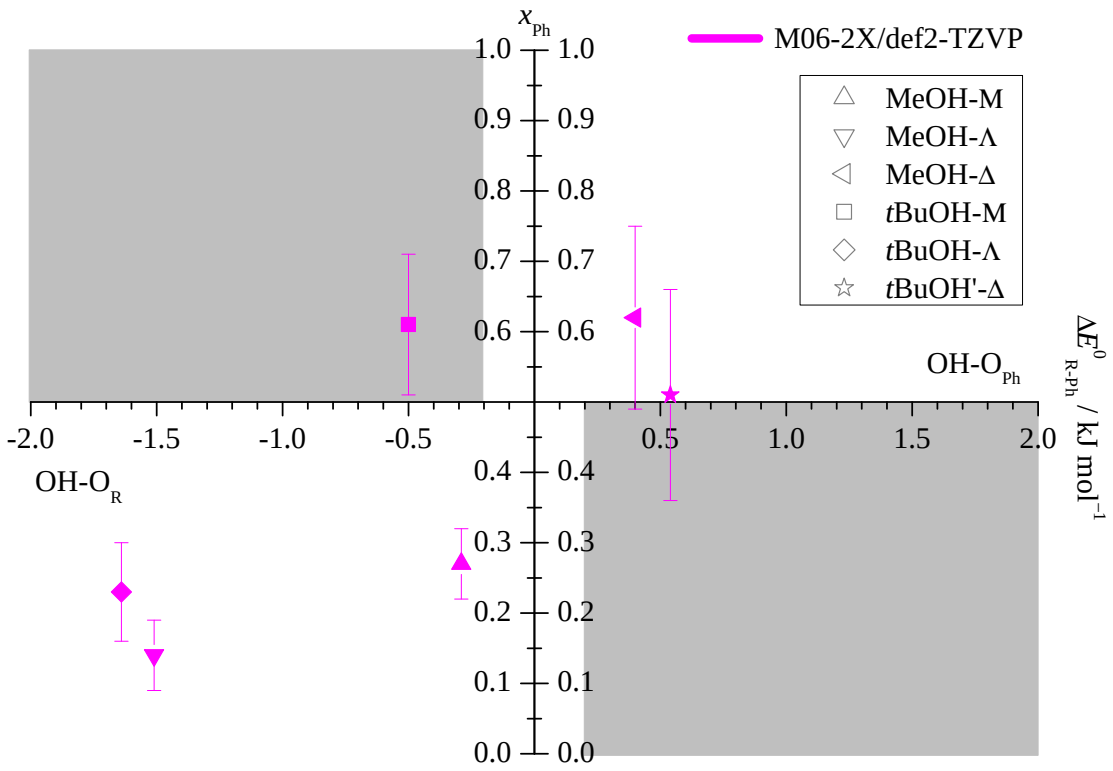

Fig. S8: Experimental fraction of phenyl docking $x_{\mathrm{Ph}} = c_{\mathrm{Ph}}/(c_{\mathrm{R}} + c_{\mathrm{Ph}})$ plotted against the M06-2X predicted ZPV corrected energy advantage for phenyl docking $\Delta E^0_{\mathrm{R-Ph}}$. Allowing for an estimated error of the ZPV correction of $\pm 0.2\,\mathrm{kJ\,mol^{-1}}$, grey areas should not fully contain data points within their indicated experimental integration error bar, if relative absorption cross sections calculated at the same level are reliable. This is the case for all systems except for *t*BuOH-M, where M06-2X predicts a slight alkyl-docking preference but the spectral intensity is consistent with more phenyl-docking.

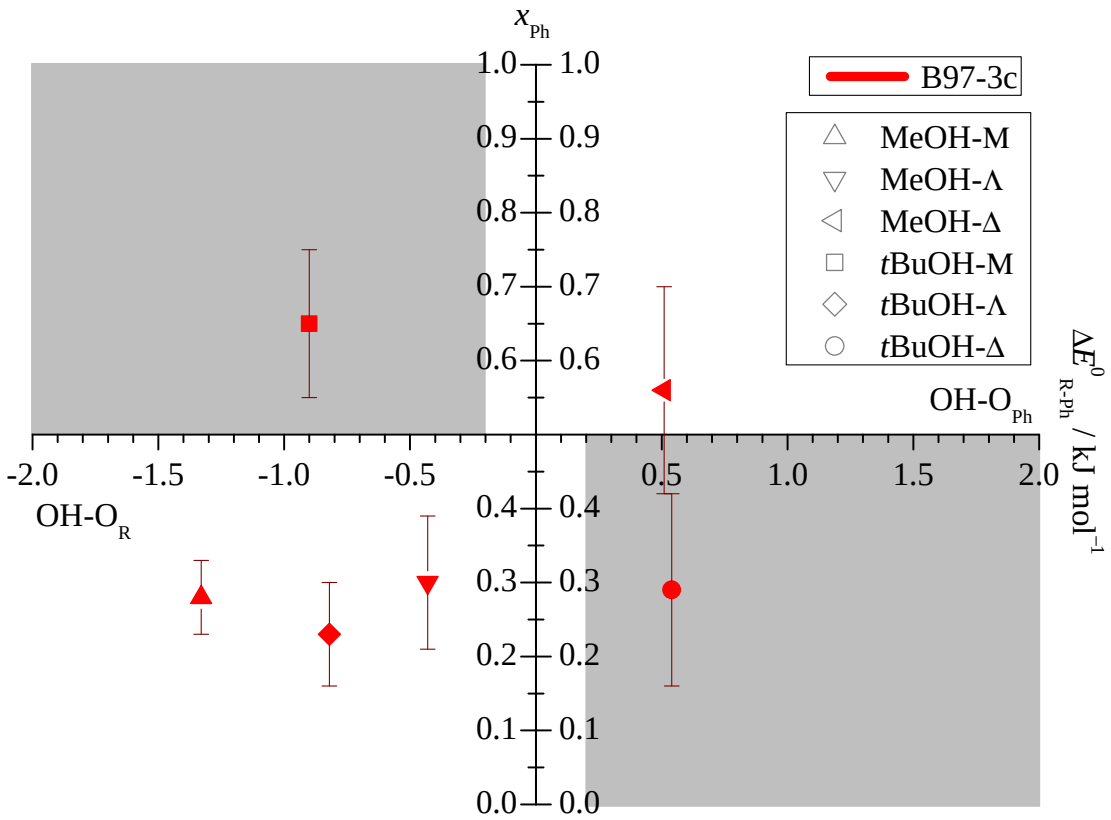

Fig. S9: Experimental fraction of phenyl docking $x_{\mathrm{Ph}} = c_{\mathrm{Ph}}/(c_{\mathrm{R}} + c_{\mathrm{Ph}})$ plotted against the B97-3c predicted ZPV corrected energy advantage for phenyl docking $\Delta E^0_{\mathrm{R-Ph}}$. Allowing for an estimated error of the ZPV correction of $\pm 0.2\,\mathrm{kJ\,mol^{-1}}$, grey areas should not fully contain data points within their indicated experimental integration error bar, if relative absorption cross sections calculated at the same level are reliable. 5 out of 6 data points reach the white areas. The *t*BuOH'-Δ structure is not predicted. Therefore, the *t*BuOH-Δ value is plotted instead.

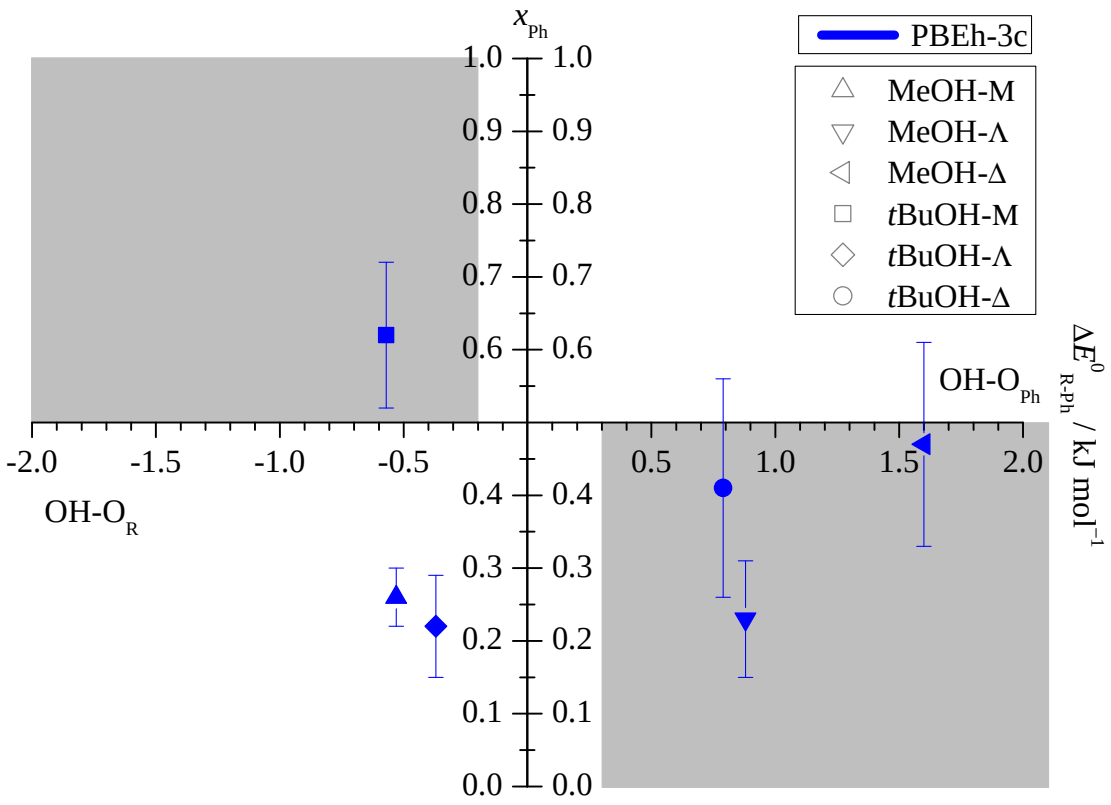

Fig. S10: Experimental fraction of phenyl docking $x_{\mathrm{Ph}} = c_{\mathrm{Ph}}/(c_{\mathrm{R}} + c_{\mathrm{Ph}})$ plotted against the PBEh-3c predicted ZPV corrected energy advantage for phenyl docking $\Delta E^0_{\mathrm{R-Ph}}$. Allowing for an estimated error of the ZPV correction of $\pm 0.2\,\mathrm{kJ\,mol^{-1}}$, grey areas should not fully contain data points within their indicated experimental integration error bar, if relative absorption cross sections calculated at the same level are reliable. 4 out of 6 data points reach the white areas. Alkyl docking is underestimated and the *t*BuOH'-Δ structure is not predicted. Therefore, the *t*BuOH-Δ value is plotted instead.

Table S4: D3 analysis in kJ mol^{-1} comparing dispersion corrections for the alkyl- vs. the phenyl-docking side at the D3-inclusive optimized structures with corresponding zero point energy correction for the B3LYP and TPSS functionals. ΔD3 in the last column gives the dispersion correction advantage for phenyl docking. A positive value means that the phenyl docking structure offers more D3 attraction than the corresponding alkyl docking structure. Out-of-plane alkyl-docking structures offer comparable or even more D3 attraction than phenyl docking. Note the strong difference between the two competing tBuOH-Δ structures. Despite its D3 alkyl-docking disadvantage, only the slightly less stable, more in-plane structure in the last row is observed experimentally along with phenyl docking. This may indicate a slight overestimation of D3 dispersion correction for this particular alkyl docking situation, which involves a cyclopropyl ring.

		With D3		Without D3		
		$\Delta E^{\mathrm{el}}_{\mathrm{R-Ph}}$	$\Delta E^{0}_{\mathrm{R-Ph}}$	$\Delta E^{\mathrm{el}}_{\mathrm{R-Ph}}$	$\Delta E^{0}_{\mathrm{R-Ph}}$	ΔD3
B3LYP-D3(BJ)	MeOH-M	-0.49	-0.64	-2.39	-2.55	$+1.9$
	MeOH-Λ	-0.10	-0.17	-1.16	-1.24	$+1.1$
	MeOH-Δ	$+1.31$	$+0.65$	-1.03	-1.70	$+2.3$
	*t*BuOH-M	-0.17	-0.23	-2.48	-2.54	$+2.3$
	*t*BuOH-Λ	-1.19	-0.91	$+0.84$	$+1.12$	-2.0
	*t*BuOH-Δ	$+0.29$	$+0.22$	$+1.32$	$+1.25$	-1.0
	*t*BuOH'-Δ	$+0.82$	$+0.61$	-3.01	-3.23	$+3.8$
TPSS-D3(BJ)	MeOH-M	-0.93	-0.98	-2.60	-2.65	$+1.7$
	MeOH-Λ	-0.07	$+0.03$	-1.21	-1.11	$+1.1$
	MeOH-Δ	$+1.09$	$+0.39$	-0.94	-1.63	$+2.0$
	*t*BuOH-M	-0.54	-0.46	-2.48	-2.41	$+1.9$
	*t*BuOH-Λ	-0.66	-0.74	$+0.66$	$+0.58$	-1.3
	*t*BuOH-Δ	$+0.32$	$+0.42$	-0.74	-0.63	$+1.1$
	*t*BuOH'-Δ	$+0.34$	$+0.55$	-4.85	-4.64	$+5.2$

Table S5: LED analysis in kJ mol^{-1} comparing dispersion corrections for the alkyl- vs. the phenyl-docking side at DLPNO-CCSD(T) level for the B3LYP and TPSS optimized minimum structures. The interfragment dispersion contributions of strong and weak pairs, as displayed in the ORCA LED output, were combined to yield the total dispersion contribution to the intermolecular interaction. ΔD in the last column gives the dispersion correction advantage for phenyl docking. A positive value means that the phenyl docking structure offers more dispersion attraction than the corresponding alkyl docking structure.

pre-optimization level		With D $\Delta E^{\mathrm{el}}_{\mathrm{R-Ph}}$	Without D $\Delta E^{\mathrm{el}}_{\mathrm{R-Ph}}$	ΔD
B3LYP-D3(BJ)	MeOH-M	-0.05	-1.92	$+1.87$
	MeOH-Λ	$+0.07$	$+0.63$	-0.56
	MeOH-Δ	$+0.88$	-0.98	$+1.86$
	*t*BuOH-M	$+0.17$	-2.08	$+2.25$
	*t*BuOH-Λ	-1.33	$+0.90$	-2.23
	*t*BuOH-Δ	$+0.06$	$+0.78$	-0.72
	*t*BuOH'-Δ	$+0.40$	-2.68	$+3.08$
TPSS-D3(BJ)	MeOH-M	-0.12	-1.63	$+1.51$
	MeOH-Λ	-0.10	$+0.18$	-0.28
	MeOH-Δ	$+0.92$	-0.80	$+1.72$
	*t*BuOH-M	$+0.12$	-1.89	$+2.01$
	*t*BuOH-Λ	-1.36	$+0.62$	-1.98
	*t*BuOH-Δ	$+0.54$	$+0.55$	-0.01
	*t*BuOH'-Δ	$+0.69$	-3.31	$+4.00$

Table S6: Energies of the two alkyl-docking isomers *t*BuOH-Δ (more out-of-plane) and *t*BuOH'-Δ (more in-plane) relative to the phenyl-docking variant for different levels of electronic structure approximation in kJ mol^{-1}. ΔE^{el} excludes and ΔE^{0} includes the harmonically approximated zero-point energy at the same level. For calculations with def2-QZVP basis and on the DLPNO-CCSD(T) level only single point energy calculations at the DFT/def2-TZVP minimized structure were carried out. Positive energy values denote a higher stability of the phenyl-docking complex. Wavenumber shifts $\Delta\omega$ relative to the phenyl-docking isomer in cm^{-1} are also given and a negative value is most consistent with experiment. No extrapolation finds *t*BuOH'-Δ to be strongly preferred but always lying very close to *t*BuOH-Δ. For B97-3c and PBEh-3c the *t*BuOH'-Δ structure is not predicted.

Method	System	$\Delta E^{\mathrm{el}}_{\mathrm{R-Ph}}$	$\Delta E^{0}_{\mathrm{R-Ph}}$	$\Delta\omega$
B3LYP-D3(BJ)	*t*BuOH-Δ	$+0.29$	$+0.22$	$+21$
def2-TZVP	*t*BuOH'-Δ	$+0.82$	$+0.61$	-15
B3LYP-D3(BJ)	*t*BuOH-Δ	$+0.01$	-	-
def2-QZVP	*t*BuOH'-Δ	$+0.39$	-	-
B3LYP-D3(BJ)//	*t*BuOH-Δ	$+0.06$	-	-
DLPNO-CCSD(T)	*t*BuOH'-Δ	$+0.40$	-	-
TPSS-D3(BJ)	*t*BuOH-Δ	$+0.32$	$+0.42$	$+28$
def2-TZVP	*t*BuOH'-Δ	$+0.34$	$+0.55$	-11
TPSS-D3(BJ)	*t*BuOH-Δ	$+0.72$	-	-
def2-QZVP	*t*BuOH'-Δ	$+0.64$	-	-
TPSS-D3(BJ)//	*t*BuOH-Δ	$+0.54$	-	-
DLPNO-CCSD(T)	*t*BuOH'-Δ	$+0.69$	-	-
M06-2X	*t*BuOH-Δ	$+0.21$	$+0.51$	$+40$
def2-TZVP	*t*BuOH'-Δ	-0.09	$+0.54$	-2
B97-3c	*t*BuOH-Δ	$+0.41$	$+0.54$	$+37$
PBEh-3c	*t*BuOH-Δ	$+1.11$	$+0.79$	-4

Table S7: Electronic dissociation energies of ketone-alcohol complexes into monomers for different DFT functionals in $\mathrm{kJ\,mol^{-1}}$. Through-bond and intermolecular effects are of comparable magnitude and the imbalance of the two docking alternatives never exceeds 5%.

Acceptor	Method	MeOH		*t*BuOH	
		R	Ph	R	Ph
M	B3LYP-D3(BJ)	33.2	32.7	33.8	33.6
	TPSS-D3(BJ)	32.2	31.2	32.3	31.7
	M06-2X	30.3	29.8	31.2	30.3
Λ	B3LYP-D3(BJ)	33.3	33.2	35.6	34.4
	TPSS-D3(BJ)	31.5	31.5	33.3	32.6
	M06-2X	31.5	30.0	33.0	31.3
Δ	B3LYP-D3(BJ)	33.3	34.7	35.1	35.4
	TPSS-D3(BJ)	31.8	32.9	32.9	33.2
	M06-2X	30.4	31.4	31.6	31.8
'-Δ	B3LYP-D3(BJ)			34.6	35.4
	TPSS-D3(BJ)			32.8	33.2
	M06-2X			31.9	31.8

Table S8: Alkyl coordination energies of acetophenone derivative/MeOH and *t*BuOH complexes predicted by different DFT methods and the corresponding single point calculations on DLPNO-CCSD(T) level in $\mathrm{kJ\,mol^{-1}}$ relative to the phenyl coordination. ΔE^{el} excludes and ΔE^{0} includes the harmonically approximated zero-point energy at DFT level. Positive energy differences denote a higher stability of the complex where the solvent docks on the phenyl side. The CCSD(T) corrections are always below $1\,\mathrm{kJ\,mol^{-1}}$ and typically below $0.5\,\mathrm{kJ\,mol^{-1}}$

Acceptor	Method	MeOH		*t*BuOH	
		$\Delta E^{\mathrm{el}}_{\mathrm{R-Ph}}$	$\Delta E^{0}_{\mathrm{R-Ph}}$	$\Delta E^{\mathrm{el}}_{\mathrm{R-Ph}}$	$\Delta E^{0}_{\mathrm{R-Ph}}$
M	B3LYP-D3(BJ)	-0.49	-0.64	-0.17	-0.23
	DLPNO-CCSD(T)//B3LYP-D3(BJ)	-0.05	-	$+0.17$	-
	TPSS-D3(BJ)	-0.93	-0.98	-0.54	-0.46
	DLPNO-CCSD(T)//TPSS-D3(BJ)	-0.12	-	$+0.12$	-
Λ	B3LYP-D3(BJ)	-0.10	-0.17	-1.19	-0.91
	DLPNO-CCSD(T)//B3LYP-D3(BJ)	$+0.07$	-	-1.33	-
	TPSS-D3(BJ)	-0.07	$+0.03$	-0.66	-0.74
	DLPNO-CCSD(T)//TPSS-D3(BJ)	-0.10	-	-1.36	-
Δ	B3LYP-D3(BJ)	$+1.31$	$+0.65$	$+0.29$	$+0.22$
	DLPNO-CCSD(T)//B3LYP-D3(BJ)	$+0.88$	-	$+0.06$	-
	TPSS-D3(BJ)	$+1.09$	$+0.39$	$+0.32$	$+0.42$
	DLPNO-CCSD(T)//TPSS-D3(BJ)	$+0.92$	-	$+0.54$	-
'-Δ	B3LYP-D3(BJ)			$+0.82$	$+0.61$
	DLPNO-CCSD(T)//B3LYP-D3(BJ)			$+0.40$	-
	TPSS-D3(BJ)			$+0.34$	$+0.55$
	DLPNO-CCSD(T)//TPSS-D3(BJ)			$+0.69$	-

References

(S1) Neese, F. *WIREs Comput. Mol. Sci.* **2018**, *8*, e1327.

(S2) Neese, F. *WIREs Comput. Mol. Sci.* **2012**, *2*, 73–78.

(S3) Frisch, M. J.; Trucks, G. W.; Schlegel, H. B.; Scuseria, G. E.; Robb, M. A.; Cheeseman, J. R.; Scalmani, G.; Barone, V.; Petersson, G. A.; Nakatsuji, H.; Li, X.; Caricato, M.; Marenich, A. V.; Bloino, J.; Janesko, B. G.; Gomperts, R.; Mennucci, B.; Hratchian, H. P.; Ortiz, J. V.; Izmaylov, A. F.; Sonnenberg, J. L.; Williams-Young, D.; Ding, F.; Lipparini, F.; Egidi, F.; Goings, J.; Peng, B.; Petrone, A.; Henderson, T.; Ranasinghe, D.; Zakrzewski, V. G.; Gao, J.; Rega, N.; Zheng, G.; Liang, W.; Hada, M.; Ehara, M.; Toyota, K.; Fukuda, R.; Hasegawa, J.; Ishida, M.; Nakajima, T.; Honda, Y.; Kitao, O.; Nakai, H.; Vreven, T.; Throssell, K.; Montgomery, J. A., Jr.; Peralta, J. E.; Ogliaro, F.; Bearpark, M. J.; Heyd, J. J.; Brothers, E. N.; Kudin, K. N.; Staroverov, V. N.; Keith, T. A.; Kobayashi, R.; Normand, J.; Raghavachari, K.; Rendell, A. P.; Burant, J. C.; Iyengar, S. S.; Tomasi, J.; Cossi, M.; Millam, J. M.; Klene, M.; Adamo, C.; Cammi, R.; Ochterski, J. W.; Martin, R. L.; Morokuma, K.; Farkas, O.; Foresman, J. B.; Fox, D. J. Gaussian 09 Revision E.01. 2016; Gaussian Inc. Wallingford CT.

(S4) TURBOMOLE V7.3 2018, a development of University of Karlsruhe and Forschungszentrum Karlsruhe GmbH, 1989-2007, TURBOMOLE GmbH, since 2007; available from `http://www.turbomole.com`.

(S5) Furche, F.; Ahlrichs, R.; Hättig, C.; Klopper, W.; Sierka, M.; Weigend, F. *WIREs Comput. Mol. Sci.* **2014**, *4*, 91–100.